INTERFACIAL REACTION OF CeO_2 FILMS WITH TEXTURED Ni-ALLOY SUBSTRATES

© 2013 G. A. Dosovitskiy[1], V. A. Amelichev[2], S. V. Samoilenkov[2], D. Eyidi[3], B. Lacroix[3], F. Paumier[3], D. P. Rodionov[4], R. J. Gaboriaud[3], A. R. Kaul[1,2]

[1]*Chemistry Department, Moscow State University, Leninskie Gory, 1/3, 119991 Moscow, Russia*

[2]*SuperOx Company, 143420 Moscow Region, Russia*

[3]*Pole Polytechnique de Recherche en Ingeniérie, Matériaux et Energétique, Boulevard M. et P. Curie, BP 30179—86962, Chasseneuil CEDEX, France*

[4]*Institute of Metals Physics, Ural branch of RAS, S. Kovalevskaya str. 18, 620041 Ekaterinburg, Russia*
e-mail: george.dos@gmail.com

Received 10.04.2013

Abstract. CeO_2 films were deposited on biaxially textured tapes of Ni-W and Ni-Cr-W alloys using MOCVD at 550 °C and subsequently treated in post-deposition annealing at 1000 °C and reducing atmosphere. Upon annealing of the films on the Ni-W alloy substrate, cube texture in the CeO_2 films was formed, and the oxide had an epitaxial interface with the Ni-W alloy substrate as shown by high resolution transmission electron microscopy. Similar annealing of the CeO_2 films on the Ni-Cr-W alloy substrate resulted in interaction of the oxide layer with the metal substrate leading to the formation of epitaxial NiO interlayer at the CeO_2/Ni-Cr-W interface.

Keywords: alloys, oxides, thin films, interfaces, chemical vapor deposition (CVD), epitaxial growth, annealing, electron microscopy, recrystallization, phase equilibria.

INTRODUCTION

Oxide films deposited onto textured metal substrates find application in the technology of high temperature superconducting (HTS) tapes based on $RBa_2Cu_3O_{7-x}$ superconductors (R – rare earth element). The crucial requirement to making HTS materials with high critical current is to ensure oriented growth of HTS films, where all grains of the superconductor layer are crystallographically aligned with each other [1]. One of the most promising approaches to HTS tape fabrication is the RABiTS technology (Rolling Assisted Biaxially Textured Substrates) [2]. Typically, epitaxial oxide buffer layers are deposited onto a metal substrate with {100} <010> biaxial texture, followed by the deposition of an epitaxial $RBa_2Cu_3O_{7-x}$ (RBCO) superconducting layer. This approach has been adopted by American Superconductor Corporation for industrial production of HTS tapes [3].

Metal substrates made of non-magnetic alloys are of great interest because they allow avoiding hysteretic losses in AC applications of HTS tapes [4]. The $Ni_{95}W_5$ alloy, which is most widely used for RABiTS, has the Curie temperature (T_C) of 320 K [5], while in Ni-Cr alloys T_C could be reduced to 0 K and cube annealing texture can still be achieved [6]. Recently, there has been certain success in preparing Ni-W alloy biaxially textured tapes with W content up to 9 at.% [7] with a T_C near 77 K, which is the highest temperature for practical applications of HTS tapes [8].

Ternary Ni-Cr-W alloys can be used for making non-magnetic substrates, since they combine several advantages such as sharp cubic annealing texture, mechanical strength and low T_C [9, 10]. However, one should take into account that Cr_2O_3 is stable at a much lower p (O_2) than WO_3 or NiO [11], so Cr-containing substrates get oxidized much easier at early stages of film growth than the pure Ni or conventional $Ni_{95}W_5$ substrates. This significantly limits suitable deposition conditions for oxide film growth on the Cr-containing metal alloy substrates.

Among many possible buffer layer materials, CeO_2 provides good crystal lattice match with the $YBa_2Cu_3O_{7-x}$ superconductor [3]. There are considerations that crack-free CeO_2 layers with a thickness over 100 nm can serve as a single buffer layer, thus significantly simplifying the RABiTS technology, where three or more buffer layers are typically used [12, 13]. Epitaxial CeO_2 films on Ni-alloy textured substrates have been obtained by various techniques, such as thermal evaporation [12], magnetron reactive sputtering [14],

laser ablation [15], and solution deposition [13, 16]. It has been shown that *c*(2x2) surface superstructure consisting of sulfur atoms on top of the (001) Ni plane is important for the oxide epitaxial growth [15]. Some approaches include high temperature annealing of non-oriented or partially oriented as-deposited CeO_2 films in the presence of O_2 or H_2O vapor in order to develop sharp cube texture. Among these are in-situ post-annealing texturing (IPAT) [17], electrodeposition [18] and solution deposition techniques [13, 16].

Metal-organic chemical vapor deposition (MOCVD) is a suitable technique for the deposition of continuous CeO_2 layers onto Ni-alloy long tapes [19], the commonly used precursor being $Ce(tmhd)_4$ ($tmhd = [(CH_3)_3C—CO-CH-CO-C(CH_3)_3]^-$). Epitaxial CeO_2 films on YSZ single crystal substrates have been grown by MOCVD using various other precursors [20], however, the growth rate in that case did not exceed 60 nm/hour. Some promising results were shown recently [21] in high growth rate laser assisted MOCVD of CeO_2 on sapphire substrates. Experiments on CeO_2 deposition onto single crystal substrates STO and YSZ showed that the increase of substrate temperature and $p(O_2)$ during the deposition helps the formation of a sharp (100) out-of-plane texture [22]. At the same time, in ref. [23] authors described the optimization of substrate temperature (462 °C) and p (O_2) (~2.1 mbar) for the deposition of {100} <011> oriented CeO_2 layers onto a Ni textured substrate, but the resulting layer texture was not sharp enough. Sharp cube textured CeO_2 layers on Ni and Ni-alloy substrates were obtained using either deposition temperature above 800 °C [19] or $p(O_2)$ above 3 mbar [24, 25]. Such conditions are not suitable for the deposition onto Cr-containing alloy substrates prone to surface oxidation.

In this work we obtained CeO_2 films using low-temperature MOCVD on the $Ni_{95}W_5$ and $Ni_{88.6}Cr_{9.2}W_{2.4}$ biaxially textured alloy substrates, and studied the processes taking place in the films during post-deposition annealing.

EXPERIMENTAL

We used $Ni_{95}W_5$ biaxially textured substrates produced by Plansee GmbH (Germany) and $Ni_{88.6}Cr_{9.2}W_{2.4}$ biaxially textured substrates produced by SuperOx (Russia). The MOCVD growth of CeO_2 films was conducted in a laboratory scale deposition system with a hot wall reactor (Fig. 1). $Ce(tmhd)_4$ was used as precursor, and its vapors were supplied into the reactor using a continuous feeding and evaporation system. The deposition system had the reel-to-reel tape transport capability, allowing the deposition of films onto moving tape. Typically we used 5 cm long pieces of substrate tapes, which were spot-weld spliced into reels of long transport tape. The deposition was carried out at 550 °C, in the atmosphere of Ar + 10 % H_2 at a total pressure of 15 mbar. Water vapor was injected into the reactor to facilitate the precursor hydrolysis; the water vapor pressure was maintained at around 0.5 mbar. After the deposition, the films were annealed at 1000 °C in the Ar + 10 % H_2 atmosphere at 5 mbar for 1 hour.

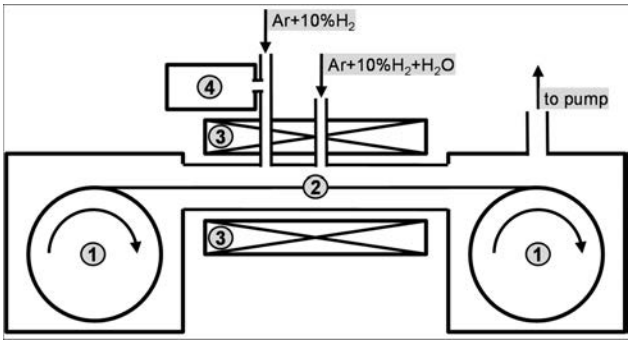

Fig. 1. MOCVD system used for the deposition of CeO_2 films: 1 — reels with metal alloy substrate tape; 2 –substrate tape; 3 — reactor furnace; 4 — precursor feeding system

Film texture was characterized using X-ray diffraction (XRD) θ-2θ scans and pole figures recorded with Rigaku SmartLab diffractometer, using Cu K_α, $\lambda = 0.154$ nm. Electron backscatter diffraction (EBSD) for orientation mapping was performed using JSM 840A Jeol scanning electron microscope with EBSD Channel 5 analyzer (HKL Technology). Transmission electron microscopy (TEM) studies including high resolution transmission electron microscopy (HRTEM) were also performed. Cross sectioned samples for TEM were prepared in the conventional way by the mechanical thinning and ion milling procedure. The samples were observed using Jeol 2200FS high resolution transmission electron microscope equipped with field emission gun operated at 200 kV. Images were taken in the bright field and dark field TEM modes, as well as in the HRTEM mode. Image processing, including Fourier transforms, was performed using Digital Micrograph software.

RESULTS

X-ray diffraction

Pole figures of the Ni-alloy substrates are shown in Fig. 2; they evidence sharp biaxial {100} <010> texture for both $Ni_{95}W_5$ and $Ni_{88.6}Cr_{9.2}W_{2.4}$ substrates.

θ-2θ XRD patterns of as-deposited CeO_2 films on both substrates show mixed orientation, containing mainly (100) and (111) components, with small part

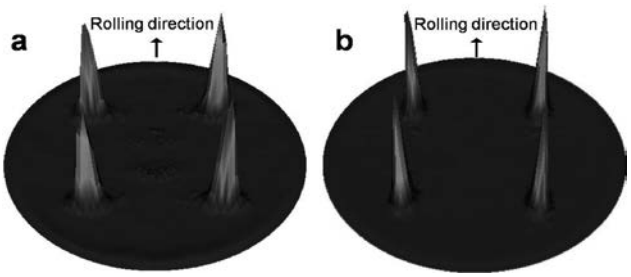

Fig. 2. (111) pole figures of $Ni_{95}W_5$ (a) and $Ni_{88.6}Cr_{9.2}W_{2.4}$ (b) alloy substrates

of (110) and (311) orientations (Fig. 3*a*, *b*) [26]. After additional annealing at 1000 °C, pure (100) texture was formed in the film on the $Ni_{95}W_5$ substrate (Fig. 3*c*), obviously due to the recrystallization of CeO_2. The out-of-plane misorientation was 9.0° in the rolling direction and 14.0° in the transversal direction, according to the rocking curves of the CeO_2 (200) plane; the in plane misorientation was 9.9° and 13.2°, respectively, according to the φ-scan of the CeO_2 (111) plane. XRD patterns of the films on the $Ni_{88.6}Cr_{9.2}W_{2.4}$ substrate after annealing (Fig. 3*d*) were taken without monochromator for higher X-ray intensity. The patterns contained substrate peaks: Ni (200) peak, its satellites due to Cu K_β and W L_α radiation of the X-ray source, and Ni (111) peak; CeO_2 peaks corresponding to the (200), (111), (220), and (311) planes; $CeCrO_3$ peaks corresponding to the (100), (110), (111), (200), and (211) planes [27]; peaks corresponding to the WO_2 (011) plane [28] and hexagonal modification of WO_3

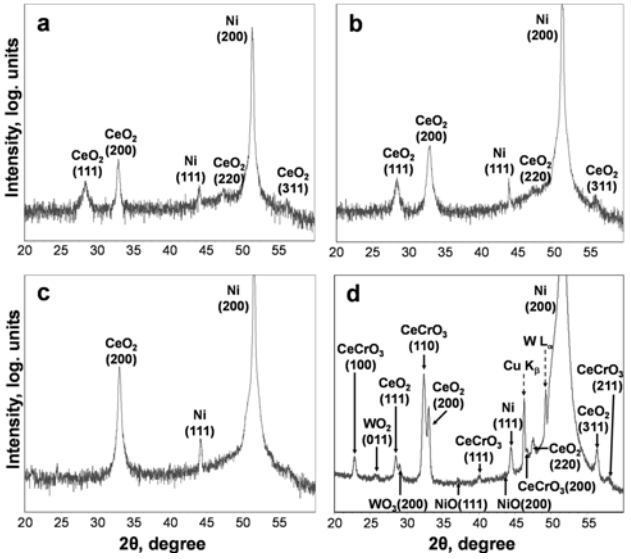

Fig. 3. θ-2θ XRD patterns of CeO_2 films: *a*) on $Ni_{95}W_5$ substrate and *b*) on $Ni_{88.6}Cr_{9.2}W_{2.4}$ substrate right after the deposition; *c*) on $Ni_{95}W_5$ substrate and *d*) on $Ni_{88.6}Cr_{9.2}W_{2.4}$ substrate after post-deposition annealing at 1000 °C

(200) [29]; as well as two weak peaks corresponding to the NiO (111) and (200) planes [30].

EBSD and TEM of CeO_2 / $Ni_{95}W_5$ films

According to EBSD data, after annealing at 1000 °C the CeO_2 layer on the $Ni_{95}W_5$ substrate contained over 97% of cube textured grains with {100} <011> orientation relative to the substrate. As it can be seen from the orientation map in Fig. 4 *a*, the CeO_2 layer consisted of 10—20 μm orientation domains that matched the size and shape of the substrate grains (Fig. 4*b*), indicating that the CeO_2 domains inherit

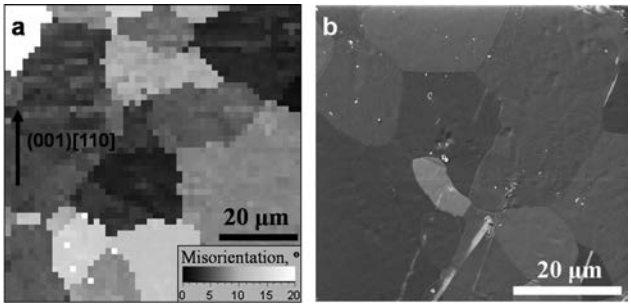

Fig. 4. *a*) EBSD orientation map of a cube-textured CeO_2 film on the $Ni_{95}W_5$ substrate; image edge is parallel to the tape rolling direction. Misorientation relative to the (001) [110] direction is shown. *b*) SEM picture of the surface of the $Ni_{95}W_5$ cube-textured substrate.

the orientation of the underlying substrate grains. In dark-field TEM images (Fig. 5) a 100 nm thick CeO_2 layer with no sharp grain boundaries could be seen (Fig. 5), suggesting that the orientation domains had no coarse grain structure. However, we observed some contrast variations in the TEM image as well as on the orientation map, which we attributed to the fine grain structure of the orientation domains, where each domain was composed of many crystallites separated by low-angle boundaries.

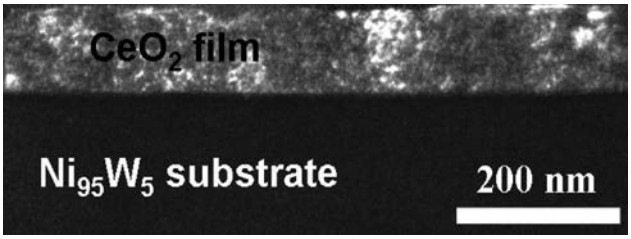

Fig. 5. TEM dark field cross-section image of a CeO_2 film on the $Ni_{95}W_5$ substrate.

CeO_2 and $Ni_{95}W_5$ formed a sharp and clear semi-coherent interface with no signs of interaction (Fig. 6*a*). Fast Fourier transform (FFT) from the substrate area

represented an fcc lattice with the [100] zone axis (Fig. 6*b*), while the FFT from the film area corresponded to an fcc lattice with the [110] zone axis (Fig. 6*c*); it was the evidence for the CeO_2 {100} <011>|| {100} <010> Ni epitaxial relations.

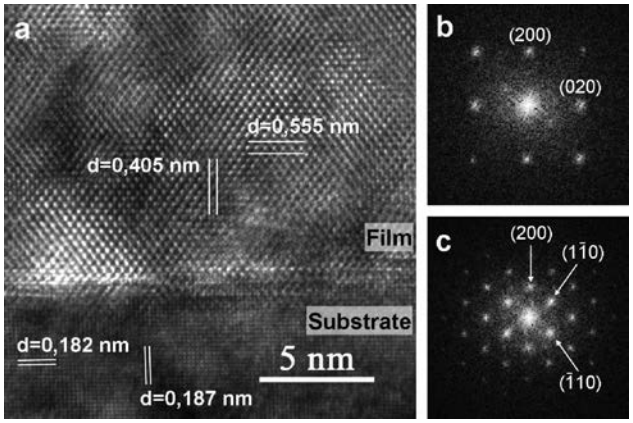

Fig. 6. *a*) HRTEM image of the $CeO_2/Ni_{95}W_5$ interface, *b*) substrate area FFT, *c*) film area FFT

TEM of $CeO_2/Ni_{88.4}Cr_{9.2}W_{2.4}$ films

TEM image of the CeO_2 film on the $Ni_{88.6}Cr_{9.2}W_{2.4}$ substrate after annealing at 1000 °C (Fig. 7) showed a strong contrast heterogeneity caused by phase heterogeneity.

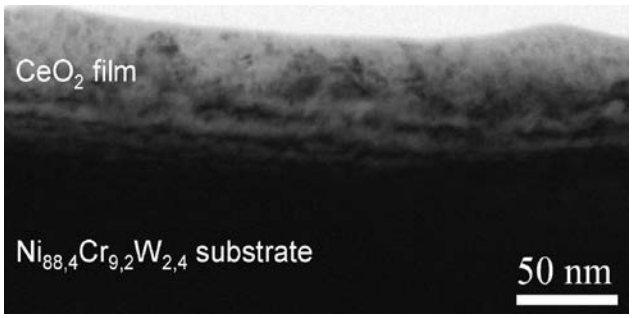

Fig. 7. TEM bright field image of the $CeO_2/Ni_{88.4}Cr_{9.2}W_{2.4}$ interface

The electron diffraction pattern of the interface area (Fig. 8) contained two sets of reflections corresponding to two co-oriented fcc lattices. One set of reflections corresponded to the $Ni_{88.6}Cr_{9.2}W_{2.4}$ alloy with a calculated lattice parameter of 0.348 nm. The other set had a lattice parameter of 0.418 nm and was ascribed to NiO, and the following epitaxial relations were established: NiO {100} <010>|| {100} <010> Ni. The NiO reflections were slightly elongated in the tangential direction, revealing certain level of misalignment of the epitaxial NiO grains. The ring of reflections corresponding to the CeO_2 {111} diffracting planes (with a calculated interplanar distance of 0.315 nm), which could also be seen on the diffraction pattern, was induced by the randomly oriented CeO_2 layer. Several reflections marked in Fig. 8 with small circles originated due to double diffraction from the $Ni_{88.6}Cr_{9.2}W_{2.4}$ and NiO lattices. It could be seen from the dark-field images (Fig. 8) that the NiO layer was located between the substrate and the CeO_2 layer. The diffraction pattern taken from the bulk of the film also demonstrated spots, which we identified as non-oriented polycrystalline CeO_2 and $CeCrO_3$.

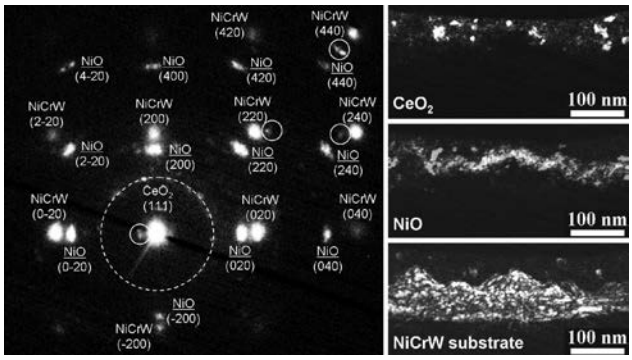

Fig. 8. Electron diffraction from the $CeO_2/Ni_{88.4}Cr_{9.2}W_{2.4}$ interface. Dashed circle marks the reflections of non-oriented CeO_2. Marked with small circles are reflections due to double diffraction. Dark-field images of the substrate, CeO_2 film, and NiO interlayer are presented on the right

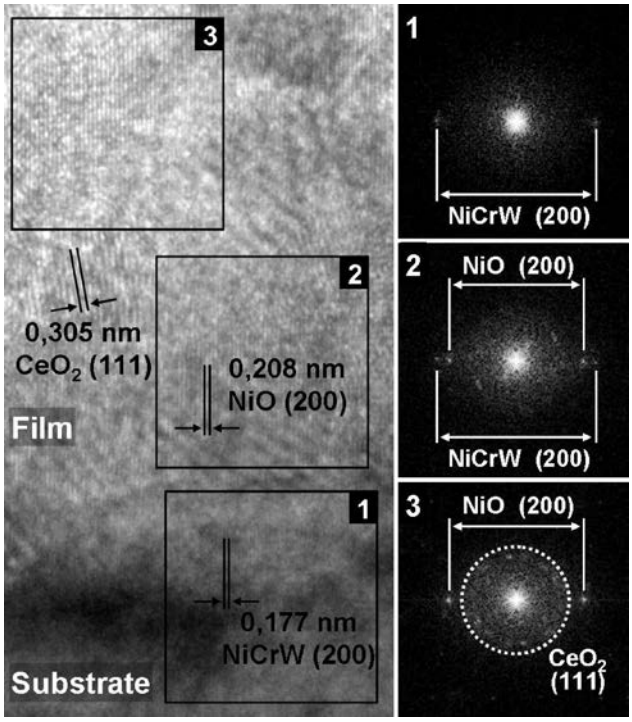

Fig. 9. HRTEM image of the $CeO_2/Ni_{88.4}Cr_{9.2}W_{2.4}$ interface (left) and FFT's of different regions (right)

We measured a number of interplanar distances on HRTEM images (Fig. 9), which corresponded to $Ni_{88.6}Cr_{9.2}W_{2.4}$ (200), NiO (200), CeO_2 (111), CeO_2 (200), and CeO_2 (220). HRTEM results confirmed that the NiO layer grew epitaxially on the $Ni_{88.6}Cr_{9.2}W_{2.4}$ substrate and separated it from the CeO_2 buffer layer.

DISCUSSION

The crystal lattice misfit values for the growth of CeO_2 on the $Ni_{95}W_5$ and $Ni_{88.6}Cr_{9.2}W_{2.4}$ substrates are 7.8% and 7.9%, respectively. Despite this relatively large mismatch, heteroepitaxial recrystallization took place in CeO_2 on $Ni_{95}W_5$ after annealing at 1000 °C, whereby CeO_2 acquired epitaxial orientation, as proved by XRD and TEM. Analogous epitaxial recrystallization of CeO_2 upon post-deposition high temperature annealing had been demonstrated earlier for CeO_2 films on single-crystal R-cut Al_2O_3 substrates [31]. At the same time, when we annealed CeO_2 films on the $Ni_{88.4}Cr_{9.2}W_{2.4}$ substrates in reducing atmosphere (Ar + 10% H_2), substrate oxidation took place leading to the formation of the NiO reaction layer while the CeO_2 layer remained poorly oriented.

The formation of the NiO layer at the interface of CeO_2 and Ni-alloy has been described in the literature for laser deposited films [32, 33]. The authors in ref. [32] used the Ni-Cr-W and Ni-Fe alloys as substrate materials, and determined the NiO layer on the Ni-Cr-W substrate by analyzing FIB images, although no NiO diffraction peaks were revealed by XRD. Pure Ni substrate was used in ref. [33]; the authors showed by TEM that the NiO layer inherited the substrate texture. The authors of both papers concluded that NiO formed not during the deposition of the CeO_2 layer itself, but during the deposition of subsequent layers, which was carried out under oxidizing conditions. Oxygen could reach the metal substrate by either solid state diffusion through the CeO_2 layer due to the high oxygen diffusivity of CeO_2 [34], or gas diffusion through microcracks in the CeO_2 layer. In ref. [35] the authors reported the formation of NiO and $NiWO_4$ at the interface between the textured Ni-W alloy substrate and the Y_2O_3 buffer layer. The authors suggested substrate oxidation during the YBCO layer processing under oxidizing conditions to be the most likely cause of that behavior.

In this work we performed the CeO_2 deposition on the Ni-W and Ni-Cr-W alloy substrates and the post-deposition film annealing under strongly reducing conditions. We found no traces of the $Ni_{95}W_5$ substrate oxidation, while the oxides of all metal substrate components were found when CeO_2 on the $Ni_{88.4}Cr_{9.2}W_{2.4}$ substrate was annealed. The key difference between the two substrates is the presence of Cr in the Ni-Cr-W alloy, whereas Cr forms an oxide at a much lower $p(O_2)$ than Ni and W (Table 1).

Table 1. Equilibrium oxygen pressure for metal oxide formation. Cr and W are considered as parts of alloys. The equilibrium oxygen pressure of oxygen-deficient cerium dioxide is provided as well

Equilibrium	at 550 °C	at 1000 °C	Reference
Ni/NiO $p(O_2)$ (bar)	$4\cdot10^{-22}$	$4\cdot10^{-11}$	[11]
$Ni_{90}Cr_{10}/Cr_2O_3$ $p(O_2)$ (bar)	$1\cdot10^{-36}$	$3\cdot10^{-20}$	[11]
$Ni_{95}W_5/WO_3$ $p(O_2)$ (bar)	$4\cdot10^{-24}$	$5\cdot10^{-10}$	[29]
$CeO_{1.9}$ equilibrium $p(O_2)$ (bar)		$1\cdot10^{-15}$	[36]

The oxidation of the Ni-Cr-W substrate could occur for any or all of the three following reasons: (1) oxygen ion diffusion through the CeO_2 layer, or (2) oxygen gas diffusion through microcracks in the CeO_2 layer, or (3) direct reaction of $Ni_{88.6}Cr_{9.2}W_{2.4}$ with CeO_2 during the annealing of the deposited layer at 1000 °C. The $p(O_2)$ generated during partial dissociation of CeO_2 is enough to oxidize chromium. The fact that no Cr_2O_3 was found in the oxidized metal substrate is in accordance with findings of Leonov et al. [37] that CeO_2 and Cr_2O_3 under reducing atmosphere react to form the $CeCrO_3$ perovskite. Indeed, using XRD we detected $CeCrO_3$ as the main substrate oxidation product in the CeO_2 / $Ni_{88.6}Cr_{9.2}W_{2.4}$ samples annealed at 1000 °C.

Besides the $CeCrO_3$ oxide, W and Ni oxides were also found in the $CeO_2/Ni_{88.6}Cr_{9.2}W_{2.4}$ samples. The oxygen partial pressure maintained during the sample annealing was not high enough for a direct oxidation of Ni or W, which is also supported by the fact, that no Ni or W oxidation occurred during the $CeO_2/Ni_{95}W_5$ sample annealing. We believe that Cr in the N-Cr-W alloy acted as a chemical pump, providing additional oxygen activity to enable the formation of NiO despite the low oxygen partial pressure annealing atmosphere. This process takes part at the early stage of low $p(O_2)$ oxidation of Ni-rich alloys containing chromium, and it has been described in the literature as the Dankov's model [38]. Nickel, as the major alloy component ($C_{Ni} >> C_{Cr}, C_W$), creates a higher chemical potential gradient across the thin surface oxide layer ($d\mu_{Ni} >$

$d\mu_{Cr}$, $d\mu_W$), which results in Ni being the major species in the flux of metal atoms diffusing towards the alloy surface during its oxidation. It should be noted that the NiO layer grew epitaxially on the metal substrate, therefore, it must have gained some additional thermodynamic stability due to the epitaxial stabilization, which lowers the $p(O_2)$ limit for its equilibrium formation, as it happens, for instance, in $RNiO_3$ (R = Pr, Nd, Sm, and Gd) on perovskite substrates [39]. This consideration could explain why NiO was located at the metal-oxide interface.

CONCLUSIONS

We have succeeded in transforming polycrystalline CeO_2 films with mixed orientation on textured Ni-alloy substrates into high-quality epitaxial films using recrystallization annealing at 1000 °C. This approach worked well on the $Ni_{95}W_5$ alloy substrates, where no film-substrate interaction was detected and a perfect {100} <010> texture developed in the CeO_2 layer. In the experiments with the $Ni_{88.6}Cr_{9.2}W_{2.4}$ alloy substrates, which contained easily oxidizing Cr, the substrates were oxidized with the formation of NiO epitaxial layer at the interface and $CeCrO_3$ as the main film-substrate interaction product.

Acknowledgements

We acknowledge the financial support from the Ministry of Education and Science of the Russian Federation under contract No. 16.523.11.3008.

REFERENCES

1. *Hilgenkamp H., Mannhart J.* // Rev. Mod. Phys. 2002. V. 74. P. 485—549.

2. *Goyal A., Norton D. P., Budai J. D. et al.* // Appl. Phys. Lett. 1996. V. 69. P. 1795—1797.

3. *Rupich M. W., Li X., Thieme C. et al.* // Supercond. Sci. Technol. 2010. V. 23. P. 014015.

4. *Clem J. R., Malozemoff A. P.* // Supercond. Sci. Technol. 2010. V. 23. P. 034014.

5. Sarma V. S., Eickemeyer J., Mickel C. et al. // Mater. Sci. Eng. A. 2004. V. 380. P. 30—33.

6. *Rodionov D. P., Gervasyeva I. V., Khlebnikova Yu.V. et al.* // Phys. Met. Metallogr. 2002. V. 93. P. 458—464.

7. *Eickemeyer J., Hühne R., Güth A. et al.* // Supercond. Sci. Technol. 2010. V. 23. P. 085012.

8. *Sarma V. S., Eickemeyer J., Schultz L. et al.* // Scripta Mater. 2004. V. 50. P. 953—957.

9. *Rodionov D. P., Dosovitskiy G. A., Kaul A. R. et al.* // Phys. Met. Metallography. 2010. V. 109. P. 632—642.

10. *Tuissi A., Villa E., Zamboni M. et al.* // Physica C. 2002. V. 372—376. P. 759—762.

11. *Richardson F. D., Jeffes J. H.E.* // J. Iron Steel Inst. 1948. V. 160. P. 261—270.

12. *Gianni L., Baldini A., Bindi M. et al.* // Physica C. 2005. V. 426—431. P. 872—877.

13. *Li G., Pu M. H., Sun R. P., et al.* // J. Alloys Comp. 2008. V. 466. P. 429—434.

14. *Xiong J., Tao B. W., Qin W. F., et al.* // Supercond. Sci. Technol. 2008. V. 21. P. 025016.

15. *Cantoni C., Christen D. K., Goyal A. et al.* // Mat. Res. Soc. Symp. Proc. 2002. V. 689. P. E9.8.1-E9.8.6.

16. *Chen S., Wang S. S., Shi K. et al.* // Physica C. 2005. V. 419. P. 7—12.

17. *Xiong J., Chen Y., Qiu Y. et al.* // Supercond. Sci. Technol. 2006. V. 19. P. 1068—1072.

18. *Phok S., Bhattacharya R. N.* // Phys. Status Solidi A. 2006. V. 203. P. 3734—3742.

19. *Stadel O., Schmidt J., Liekefett M. et al.* // IEEE Trans. Appl. Supercond. 2003. V. 13. P. 2528—2531.

20. *Wang A., Belot J. A., Marks T. J. et al.* // Physica C. 1999. V. 320. P. 154—160.

21. *Zhao P., Ito A., Tu R. et al.* // Surf. Coat. Technol. 2011. V. 205. P. 4079—4082.

22. *Becht M., Morishita T.* // Chem. Vap. Deposition. 1996. V. 2. P. 191—197.

23. *Lee H. G., Lee Y. M., Shin H. S. et al.* // Mat. Sci. Eng. B. 2002. V. 90. P. 20—24.

24. *Kim H. J., Joo J., Ji B. K. et al.* // IEEE Trans. Appl. Supercond. 2003. V. 13. P. 2555—2558.

25. *Kim C. J., Kim H. J., Sun J. W. et al.* // Physica C. 2003. V. 386. P. 327—332.

26. *Harwood M. G.* // Nature (London). 1949. V. 164. P. 787.

27. *Wold A., Ward R.* // J. Am. Chem. Soc. 1954. V. 76. P. 1029—1030.

28. *Palmer D. J., Dickens P. G.* // Acta Crystallogr. 1979. V. B35. P. 2199—2201.

29. *Blednov A. V., Gorbenko O. Yu., Rodionov D. P. et al.* // J. Mater. Res. 2010. V. 25. P. 2362—2370.

30. *Barrett C. A., Evans E. B.* // J. Am. Ceram. Soc. 1964. V. 47. P. 533—533.

31. *Graboy I. E., Markov N. V., Maleev V. V. et al.* // J. Alloys Comp. 1997. V. 251. P. 318—321.

32. *Tomov R. I., Kursumovic A., Kang D. J. et al.* // Physica C. 2002. V. 372—376. P. 810—813.

33. *Sun E. Y., Goyal A., Norton D. P. et al.* // Physica C. 1999. V. 321. P. 29—38.

34. *Tidrow S. C., Wilber W. D., Tauber A. et al.* // J. Mater. Res. 1995. V. 10. P. 1622—1634.

35. *Leonard K. J., Goyal A., Kang S. et al.* // Supercond. Sci. Technol. 2004. V. 17. P. 1295—1302.

36. *Tretyakov Yu.D.* Chemistry of non-stoichiometric oxides (hardcover). Moscow: Lomonosov MSU press, 1974. 364 p.

37. *Leonov A. I., Andreeva A. V., Shvaiko-Shvaikovskii V.E. et al.* // Izv. Akad. Nauk SSSR, Neorg. Mater. 1966. V. 2. P. 517—523.

38. *Dankov P. D.* // J. Phys. Chem. (USSR). 1952. V. 26. P. 753—758.

39. *Novojilov M. A., Gorbenko O. Y., Graboy I. E. et al.* // Appl. Phys. Lett. 2000. V. 76. P. 2041—2043.

Dosovitskiy Georgy A. — Ph.D., Researcher at NeoChem JSC, Moscow, Russian Federation

Amelichev Vadim A. — Ph.D., Researcher at SuperOx Company, Moscow, Russian Federation

Samoilenkov Sergey V. — Ph.D., Chief Technology Officer at SuperOx Company, Moscow, Russian Federation

Eyidi Dominique — Ph.D., Researcher at Pole Polytechnique de Recherche en Ingeniérie, Matériaux et Energétique, Chasseneuil CEDEX, France

Lacroix Bertrand — Ph.D., Pole Polytechnique de Recherche en Ingeniérie, Matériaux et Energétique, Chasseneuil CEDEX, France

Paumier Fabien — Ph.D., Researcher at Pole Polytechnique de Recherche en Ingeniérie, Matériaux et Energétique, Chasseneuil CEDEX, France

Rodionov Dmitry P. — Dr.Sci., Leading Researcher at Institute of Metals Physics, Ural dpt. of RAS, Ekaterinburg, Russian Federation

Gaboriaud Rolly J. — Professor, Head of laborattory at Pole Polytechnique de Recherche en Ingeniérie, Matériaux et Energétique, Chasseneuil CEDEX, France

Kaul Andrey R. — Dr. Sci. (Chem.), Professor, Head of laborattory at Chemistry Department, Moscow State University, Moscow, Russian Federation, Chief Scientist at SuperOx Company, Moscow, Russian Federation